effects, because measurements were made upstream of the onset of intermittent backflow.

In Figs. 2 and 3, the bursting frequency f^+ has been normalized to the zero-pressure-gradient case (calculated from the average of the empty tunnel values for the current results) to highlight changes in f^+ from this baseline condition. Note the close match in trends between the data of White and Tiederman[12] and the data for the diffusing wall of the current study. Recall that the diffusing wall case, like that of White and Tiederman,[12] represents a boundary layer that is fully attached yet developing in an adverse pressure gradient. Both of these cases show a sharp rise in f^+ with increasing pressure gradient. The data for the cases approaching separation clearly do not display this feature. The increases in f^+ are more modest, and there is in general a more mild increasing trend with pressure gradient. There are few data sets in the open literature documenting boundary-layer bursting behavior for separating flows. Strickland and Simpson[7] present results that may be used for comparison, and these data (taken from the tables in Ref. 7) are plotted in Fig. 3. The data agree well with those of the strong- and mild-backflow-separation cases of the present study.

Whereas the Blackwelder data of Fig. 1 show that a mild f^+ dependence on Reynolds number exists, the data of the current experiment presented in Figs. 2 and 3 are meant to highlight the additional important effect of the pressure gradient. The pressure gradient appears to cause different responses for fully attached and separating boundary layers. Of the three separation cases presented, note the reasonably good agreement between those of the strong and mild backflows. These two cases possessed pressure distributions that were similar in character. The pressure distribution for the case of the backflow aerodynamic blockage differed in that changes in the pressure gradient were stronger and occurred farther along in the pressure field development. This may be responsible for some of the differences observed between this and the other separation cases.

Note that the findings of this study were unaltered upon recalculation of the bursting frequencies with the threshold detection parameter doubled. Along with the obvious result of lowering the absolute levels of f_b, the relative trends among the various flow cases were found to be unchanged. This result provides good confidence in the measured data and in the findings presented thus far.

Conclusions

It is concluded that while inner-variable scaling is a proper nondimensionalization of the turbulent-boundary-layer bursting frequency, Reynolds number alone is not sufficient to adequately describe the behavior of this parameter. The pressure distribution is necessary to aid in the interpretation of scaled-bursting-frequency results. In addition, turbulent boundary layers approaching separation exhibit a marked reduction in bursting frequency augmentation relative to fully attached boundary layers developing within an adverse pressure gradient. While the scaled bursting frequency is increased relative to zero-pressure-gradient cases, the increases are more gradual and modest than corresponding increases for the fully attached adverse-pressure-gradient boundary layers. This indicates the existence of a less active condition of the boundary layer for flows approaching separation.

References

[1]Kim, J., and Spalart, P. R., "Scaling of the Bursting Frequency in Turbulent Boundary Layers at Low Reynolds Numbers," *Physics of Fluids*, Vol. 30, No. 11, 1987, pp. 3326–3328.

[2]Luchik, T. S., and Tiederman, W. G., "Timescale and Structure of Ejections and Bursts in Turbulent Channel Flows," *Journal of Fluid Mechanics*, Vol. 174, Jan. 1987, pp. 529–552.

[3]Shiau, B. S., and Lu, S. S., "Detection of Burst-Events in the Turbulent Boundary Layer," *Journal of the Chinese Institute of Engineers*, Vol. 11, No. 2, 1988, pp. 147–153.

[4]Wei, S., and Ning, T., "Bursting Frequency in Turbulent Boundary Layer," *ACTA Mechanica Sinica*, Vol. 4, No. 4, 1988, pp. 291–296.

[5]Blackwelder, R. F., and Haritonidis, J. H., "Scaling of the Bursting Frequency in Turbulent Boundary Layers," *Journal of Fluid Mechanics*, Vol. 132, July 1983, pp. 87–103.

[6]Rao, K. N., Narasimha, R., and Narayanan, M. A. B., "The 'Bursting' Phenomenon in a Turbulent Boundary Layer," *Journal of Fluid Mechanics*, Vol. 48, Pt. 2, 1971, pp. 339–352.

[7]Strickland, J. H., and Simpson, R. L., "The 'Bursting' Frequencies Obtained from Wall Shear Stress Fluctuations in a Turbulent Boundary Layer," *Physics of Fluids*, Vol. 18, No. 3, 1975, pp. 306–308.

[8]Simpson, R. L., Strickland, J. H., and Barr, P. W., "Features of a Separating Turbulent Boundary Layer in the Vicinity of Separation," *Journal of Fluid Mechanics*, Vol. 79, Jan.–March 1977, pp. 553–594.

[9]Lu, S. S., and Willmarth, W. W., "Measurements of the Structure of the Reynolds Stress in a Turbulent Boundary Layer," *Journal of Fluid Mechanics*, Vol. 60, Pt. 3, 1973, pp. 481–511.

[10]Shah, D. A., and Antonia, R. A., "Scaling of the 'Bursting' Period in Turbulent Boundary Layer and Duct Flows," *Physics of Fluids*, Vol. 1, No. 2, 1989, pp. 318–325.

[11]Bandyopadhyay, P. R., "Period Between Bursting in Turbulent Boundary Layers," *Physics of Fluids*, Vol. 25, No. 10, 1982, pp. 1751–1754.

[12]White, J. B., and Tiederman, W. G., "The Effects of Adverse Pressure Gradient on Turbulent Burst Structure in Low-Reynolds Number Equilibrium Boundary Layers," Office of Naval Research, ONR Rept. PME-FM-90-2, Purdue Univ., West Lafayette, IN, Jan. 1990.

[13]Tillman, G., "An Experimental Study of Two-Dimensional Turbulent Boundary Layer Separation," Ph.D. Thesis, Dept. of Mechanical Engineering, Northwestern Univ., Evanston, IL, June 1994.

Drag Reduction with the Slip Wall

D. W. Bechert*
DLR, German Aerospace Research Establishment, Berlin 10623, Germany
and
W. Hage† and M. Brusek†
Technische Universität Berlin, Berlin 10623, Germany

Introduction

FOR rigid surfaces immersed in a flow, the no-slip condition on the wall holds. In simplistic terms, the basic idea of our slip wall is to release the no-slip condition to reduce drag. This is achieved with a belt that replaces the rigid wall. The moving belt, driven by the flow shear stress itself, reduces the velocity difference between mean flow and the wall, and thus it reduces the skin friction. Our device should not be confused with an actively driven belt surface like the one of a moving floor in a wind tunnel. We deal with a purely passive device. Simplified theoretical predictions show an impressive drag reduction potential. In our oil channel, we have experimentally demonstrated the feasibility of the concept. These first trials have shown a 9% net drag reduction, which is probably much less than can be achieved with a careful optimization of the system.

The idea of reducing drag by releasing the no-slip condition in some way is actually not so new. For instance, the following two drag reduction concepts are based on this idea. 1) The pressure loss in pipelines carrying highly viscous crude oil can be decreased dramatically by the injection of water.[1] The water remains close to the wall and, by its low viscosity, practically removes the no-slip condition of the crude oil at the wall. 2) Air can be ejected through the hulls of ships to reduce their drag in water.[2]

At first glance, it is not obvious that a passively moving belt can indeed reduce the wall shear stress. Therefore, to demonstrate the drag reduction capability of our slip wall we will discuss here a model that, admittedly, is at the verge of oversimplification. However, it exhibits clearly the physics of the slip wall system as well as its possible limits (Fig. 1). As a first (crude) approximation, we assume that the turbulent shear stress on the belt is proportional to

Received July 10, 1995; revision received Nov. 15, 1995; accepted for publication Jan. 29, 1996.

*Senior Scientist, Abt. Turbulenzforschung, Müller-Breslau-Str. 8. Senior Member AIAA.

†Scientist, Hermann-Föttinger-Institut für Strömungsmechanik, Strasse des 17. Juni 135.

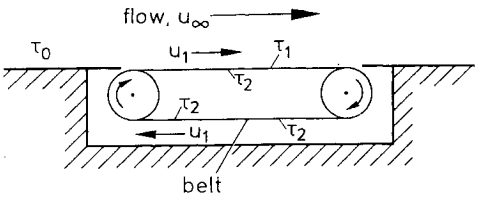

Fig. 1 Schematic of the slip wall belt arrangement.

the square of the velocity relative to the wall. In addition, we assume that only the straight parts of the belt contribute to the shear forces (Fig. 1). The shear stress τ_1 on the exposed upper surface has to drag along the other three surfaces of the belt that experience a lower shear stress τ_2. Consequently, we have $\tau_1 = 3\tau_2$ or $(u_\infty - u_1)^2 = 3u_1^2$. Thus, for the belt velocity u_1 we obtain a value of 36.6% of the mean flow velocity u_∞. The shear stress on the exposed upper belt surface is reduced to 40% of that of a rigid surface. This corresponds to 60% drag reduction. Clearly, this is a theoretical limit that cannot be met in practice. A closer inspection of Fig. 1 shows that other constituents of fluid dynamical and frictional losses of the belt system must play important roles. However, these additional losses are difficult to estimate, and the most important task in further experiments is to determine and to minimize them. Nevertheless, to bracket the size of the effect, we now assume the system losses to be 27 times (!) higher than we had assumed before. With these very substantial system losses, we find $u_1 = 0.10u_\infty$, and we still predict about 20% drag reduction. Finally, with a calculation similar to that performed earlier, we also can predict a drag reduction of the slip wall for laminar flow.

Experimental Apparatus

All tests have been conducted in the Berlin Oil Channel.[3] The shear stress measurements were carried out in a turbulent channel flow using a floating element balance. This balance compares the shear stress of the test plate with that on a smooth reference plate. In this way, an unprecedented accuracy of ±0.3% for the shear stress measurements is obtained.[3] The test plate (Fig. 2) is inserted into the channel wall. It has a surface area of 400×500 mm^2 and contains the belt device. The turbulent shear force on the exposed surface of the belt (293×328 mm^2) is typically between 0.046 and 0.36 N. This range is sufficient to get the belt motion started in our experiment. Our belt consists of a thin (0.1-mm) spring steel ribbon. The suspension wheels are actually disk arrays (Fig. 2). These disk arrays reduce the fluid dynamical losses of the belt system considerably, as compared with simple cylindrical suspension wheels. As can be seen in Fig. 2, additional supporting wheels were installed that keep the belt from fluttering. These supporting wheels were designed to attract the steel belt magnetically. This was achieved by mounting neodymium super magnets onto the steel disks of the wheels.

Our slip wall test plate is the first of its kind, and therefore it still has some technical problems that, however, are solvable and will be solved.

1) One such problem is how to keep the belt on the wheels so that it does not wander off laterally. On conventional transmissions with leather belts, a sufficient lateral guidance is obtained by a slight spherical shape of the wheels. Our disk array wheels (Fig. 2) also exhibit disks of slightly (by 0.1 mm) smaller diameter at the sides. On the other hand, our steel belt exhibits a high elastic stiffness. This causes a very high (and undesired) tension in its middle and a very low one at the sides. Thus, the belt is rather limp at its sides. The magnetical wheels partly compensate for this deficiency. In further tests, however, the belt control will be replaced by a more advanced device.

2) Quite unexpectedly, because of the very low Coulomb friction in the ball bearings of the wheels, elastic restoring forces in the belt/wheel system turned out to be a major problem. The elastic restoring forces always tend to move the belt system back to a certain position. It is this elastic restoring force (rather than the Coulomb friction) that has to be overcome when the belt system starts moving. The elastic restoring force is caused both by belt inhomogeneities, such as the end connections, and by minute eccentricities of the wheels. These eccentricities are on the order of 0.01 mm, and they are difficult to avoid. The high modulus of elasticity of the steel

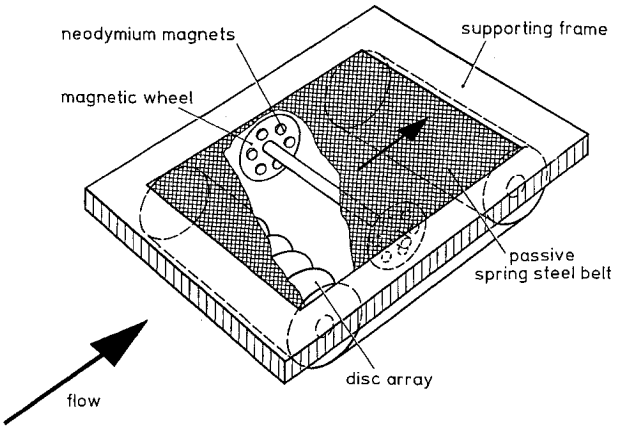

Fig. 2 Slip wall test plate.

belt aggravates the situation because minute deflections generate large restoring forces. We could somewhat alleviate the situation by installing soft elastic suspensions for the wheel bearings.

From the preceding discussion of technical problems the reader will rightly conclude that some engineering development is still required to make slip wall surfaces work both reliably and efficiently. Nevertheless, with the present setup we were able to demonstrate that the concept is viable.

Results and Conclusions

In Fig. 3, some data from our exploratory measurements can be seen. The data show shear stress reduction values in terms of $\Delta\tau/\tau_0$. In this expression we define $\Delta\tau = \tau_1 - \tau_0$. This is the (measured) shear stress τ_1, which is exerted on the exposed belt area, minus the reference shear stress τ_0 of a smooth plate being exposed to identical flow conditions. The difference $\Delta\tau$ is normalized with τ_0. Therefore, a drag reduction corresponds to negative values of $\Delta\tau/\tau_0$ in our Fig. 3. On the horizontal axis, we have plotted two quantities that may characterize the flow properties, i.e., τ_0 and Re_{ch}.The Reynolds number Re_{ch} is calculated with the average velocity $\bar{u}$ in the channel cross section and with the lateral width d of the channel; $d = 0.25$ m. The kinematic viscosity of the fluid is $\nu = 1.25 \times 10^{-5}$ m^2/s. The peak velocity at the center of the channel is about 11% higher than the average velocity $\bar{u}$ in the channel.

Figure 3 also shows a reference experiment with the steel belt being arrested. The turbulent shear stress on the arrested belt is slightly increased relative to the smooth reference wall. This is probably because of parasitic effects, such as having little gaps around the belt to prevent binding. In addition, a weak turbulence-induced wiggling motion of the belt has been noticed that may also contribute to this slightly elevated shear stress for the arrested belt. However, once the belt starts running, a significant drag reduction is observed. We have operated the belt system with higher and lower belt tension (not specified here, but both in the 100-N regime). A lower belt tension creates a lower restoring force, and thus the belt starts running at lower Reynolds number. During the measurements, it turned out that the belt speed was not as nicely constant as one might have wished. This, again, is an effect caused by the elastic restoring force that is different in different belt positions. Nevertheless, the measurements were reproducible because the data for each data point in Fig. 3 were taken over 10–20 min.

The measured belt velocity varied between 8 and 12% of the peak velocity at the center of the channel for the low belt tension condition and between 6 and 8% for the high belt tension condition. At these belt velocities, our simplistic theoretical estimation would suggest a somewhat higher drag reduction, in particular for the low belt tension condition, where a slight belt flutter was observed that we consider as a deleterious effect.

Finally, we would like to stress that the limited amount of data being provided in Fig. 3 is only intended to convince the reader that the slip wall concept really works and that it can produce an appreciable amount of drag reduction. This is not a small achievement if one considers how modest the success rate in drag reduction research has been so far and how much time and money has been spent (also in our laboratory) on concepts that finally turned out not to work.

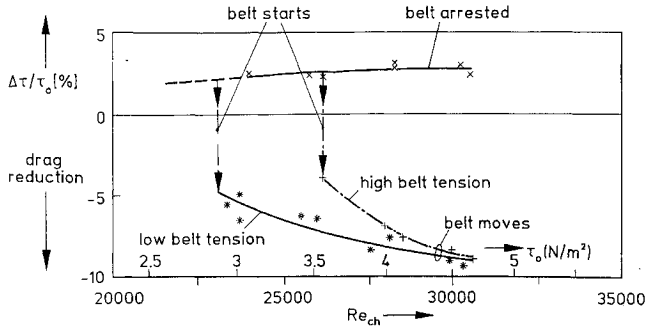

Fig. 3 Drag reduction by the slip wall.

Acknowledgments

Funding for this project has been provided by the Deutsche Forschungsgemeinschaft and is gratefully acknowledged. In addition, we thank D. R. Noergel for his comments on the manuscript.

References

[1]Joseph, D. D., and Renardy, Y. Y., *Fundamentals of Two-Fluid Dynamics, Part II: Lubricated Transport, Drops and Miscible Liquids*, Springer–Verlag, Berlin, 1993.

[2]Merkle, C. L., and Deutsch, S., "Drag Reduction in Liquid Boundary Layers by Gas Injection," *Viscous Drag Reduction in Boundary Layers*, edited by D. M. Bushnell and J. N. Hefner, Vol. 123, Progress in Astronautics and Aeronautics, AIAA, Washington, DC, 1990, pp. 351–412.

[3]Bechert, D. W., Hoppe, G., van der Hoeven, J. G. T., and Makris, R., "The Berlin Oil Channel for Drag Reduction Research," *Experiments in Fluids*, Vol. 12, 1992, pp. 251–260.

Limitations of Traditional Finite Volume Discretizations for Unsteady Computational Fluid Dynamics

J. Russell Manson*
Bucknell University, Lewisburg, Pennsylvania 17837
Gareth Pender†
Glasgow University,
Glasgow G12 8LT, Scotland, United Kingdom
and
Steve G. Wallis‡
Heriot–Watt University,
Edinburgh EH14 4AS, Scotland, United Kingdom

Introduction

TRADITIONAL finite volume methods are popular in the field of refined subsonic flow simulation. Although a degree of confidence has been established in existing algorithms for accurate steady-state simulations (at least for laminar flows), a dubiety still pervades unsteady simulations.[1] The traditional finite volume approach is typified by Patankar's SIMPLE algorithm,[2] an approach and terminology for discretizing the equations of fluid flow, heat transfer, and associated transport processes. This methodology, although adequate for steady-state simulations, is ineffective for unsteady state problems with significant convective effects. This was recognized over 15 years ago by Leonard,[3] who describes two quite different methodologies for steady- and unsteady-state problems [QUICK (quadratic upstream interpolation for convective kinematics) and QUICKEST, respectively]. The computational fluid dynamics community has largely adopted Leonard's suggestion for steady subsonic flow modeling since Patankar's discretization can be readily "QUICK"ened by simply changing the interpolation functions for the face values. The same approach is not readily extendable to unsteady simulations. It performs progressively worse as the Courant number increases beyond 1, countering the only reason for using it in preference to the computationally cheaper explicit methods.

Received Aug. 4, 1995; revision received Oct. 4, 1995; accepted for publication Nov. 10, 1995.

*Assistant Professor of Civil Engineering, Department of Civil Engineering.

†Lecturer in Civil Engineering, Department of Civil Engineering.

‡Lecturer in Civil and Offshore Engineering, Department of Civil Engineering and Offshore Engineering.

Advective Transport and Traditional Finite Volume Discretization

In one dimension unsteady convection (sometimes called advection) is represented in a conservative form by

$$\frac{\partial \phi}{\partial t} + \frac{\partial (u\phi)}{\partial x} = 0 \tag{1}$$

where ϕ is the convected variable and u the convecting velocity, taken here to be uniform, steady, and positive. Adopting the notation of Patankar, and referring to Fig. 1, the finite volume representation of Eq. (1) is given by integrating it over the control volume:

$$\int_w^e \left[\int_t^{t+\Delta t} \frac{\partial \phi}{\partial t}\, dt \right] dx = -\int_w^e \left[\int_t^{t+\Delta t} \frac{\partial u\phi}{\partial x}\, dt \right] dx \tag{2}$$

The discrete equation becomes

$$\left(\phi_P - \phi_P^0\right)\Delta x + \left\{ f[(u\phi)_e - (u\phi)_w] + (1-f)\left[(u\phi)_e^0 - (u\phi)_w^0\right] \right\} \Delta t = 0 \tag{3}$$

where f is a Crank–Nicolson temporal weighting factor. A stability analysis indicates that as long as $f \geq 0.5$, this discretization is unconditionally stable[4]; thus the choice of time step is not limited by stability considerations. In Eq. (3) the unknown values of ϕ at the future time have no superscript, whereas known values at the present time are given the 0 superscript. We may rearrange Eq. (3) as follows with all known quantities appearing on the right-hand side of the equation:

$$\phi_P + \frac{u\Delta t}{\Delta x} f(\phi_e - \phi_w) = \phi_P^0 - \frac{u\Delta t}{\Delta x}(1-f)\left(\phi_e^0 - \phi_w^0\right) \tag{4}$$

In Eq. (4), $u\Delta t/\Delta x$ is the Courant number. To complete the development, interpolation functions are required for the face values ϕ_e and ϕ_w in terms of the nodal values (ϕ_W, ϕ_P, ϕ_E, etc.). Perhaps the most intuitive interpolation for ϕ_e is given by

$$\phi_e = \tfrac{1}{2}(\phi_E + \phi_P) \tag{5}$$

whereas a more reasoned approach, which takes account of the physical argument that information travels downwind, is given by

$$\phi_e = \phi_P \tag{6}$$

Both of these simple interpolations are now widely discredited. The former method, termed central differencing, introduces too much artificial dispersion producing wiggles when individual Fourier components propagate at different celerities. The latter method, termed first-order upwinding, introduces too much artificial diffusion, which results in anomalously high spreading of initially sharp

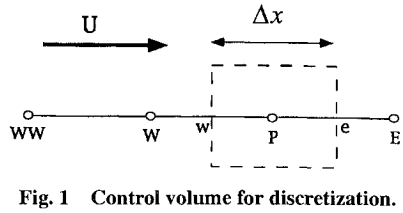

Fig. 1 Control volume for discretization.